

**Energy localization and excess fluctuations from
long-range interactions in equilibrium molecular dynamics**

Ralph V. Chamberlin

Department of Physics, Arizona State University, Tempe, AZ 85287-1504 USA

Vladimiro Mujica

School of Molecular Science, Arizona State University, Tempe, AZ 85287-1604 USA

Sergei Izvyekov and James P. Larentzos

US Army Research Laboratory, Aberdeen Proving Ground, MD 21005 USA

Abstract

Molecular Dynamics (MD) simulations of standard systems of interacting particles (“atoms”) give excellent agreement with the equipartition theorem for the average energy, but we find that these simulations exhibit finite-size effects in the dynamics that cause local fluctuations in energy to deviate significantly from the analogous energy fluctuation relation (EFR). We have made a detailed analysis of Lennard-Jones atoms to track the origin of such unphysical fluctuations, which must be corrected for an appropriate description of the statistical mechanics of small systems, especially at low temperatures (T). Similar behavior is found in a model of nitromethane at higher T . The main conclusion of our study is that systems separated into nanometer-sized “blocks” inside much larger simulations exhibit excess fluctuations in potential energy (pe) that diverge inversely proportional to T in a manner that is strongly dependent on the range of interaction. Specifically, at low T with long-range interactions pe fluctuations exceed the EFR by at least an order of magnitude, dropping abruptly to below the EFR when interactions include only 1st-neighbor atoms. Thus, excess pe fluctuations cannot be due to simple surface effects from the robustly harmonic 1st-neighbor interactions, nor from any details in the simulations or analysis. A simplistic model that includes 2nd-neighbor interactions matches the behavior of the excess pe fluctuations, but only if the 2nd-neighbor terms are not included in Boltzmann’s factor, attributable to energy localization due to anharmonic effects. Characterizing energy correlations as a function of time and distance reveals that excess pe fluctuations in a block coincide with negative pe correlations between neighboring blocks, whereas reduced pe fluctuations coincide with positive pe correlations. Indeed, anomalous pe fluctuations in small systems at low T can be quantified by using the net energy in Boltzmann’s factor that includes the pe from a surrounding shell of similarly small systems, or equivalently an effective local temperature. Our analysis elucidates the source of non-Boltzmann fluctuations, and the need to include mesoscopic thermal effects from the local environment for a consistent theoretical description of the equilibrium fluctuations in MD simulations of standard models with long-range interactions.

Keywords: statistical physics; MD simulations; fluctuations; nanoscale dynamics; specific heat; crystals

I. Introduction

Molecular dynamics (MD) simulations provide a powerful tool for studying the behavior of atoms and molecules in many models of practical importance, but they also provide idealized systems for fundamental investigations connecting classical and statistical mechanics [1-5]. In fact, the first MD simulations using a digital computer tested whether point-like particles obeying classical mechanics would reach thermal equilibrium if connected by anharmonic springs. To the surprise of Enrico Fermi and his team, these simulations showed recurrent energy cycling with no indication of the stable equipartition of energy expected for classical systems in the canonical ensemble. Now it is known that chaotic motion in large systems of interacting particles (“atoms”) allows them to reach thermal-equilibrium average behavior, but questions remain regarding the dynamics [6-10]. Here we use MD simulations of diverse models to test for canonical-ensemble behavior in the average local energies, and their fluctuations. The average energies show excellent agreement with the expected equipartition theorem, but their fluctuations often deviate from the usual energy fluctuation relation (EFR), sometimes by an order of magnitude or more. Key insight comes from energy correlations as a function of time and distance showing that deviations from this EFR can be attributed to energy that is transiently localized during equilibrium fluctuations, thereby altering the net energy that reaches distant parts of the simulation volume serving as the heat reservoir needed for the emergence of a well-defined Boltzmann’s factor. Another result is a connection between energy fluctuations and atom density due to the attractive interaction between 2nd-neighbor atoms. This interpretation is confirmed by reducing the interaction range until there are only repulsive forces between 1st-neighbor atoms, which is the only way we have found to obtain dynamics that fully agrees with the EFR.

Because conservation of total energy is intrinsic to MD simulations based solely on Newton’s laws, fluctuations in the full simulation come only from transfer between kinetic energy (*KE*) and potential energy (*PE*). (Lower-case acronyms will be reserved for when the number of particles may change, to emphasize that for local fluctuations we utilize the energy per particle.) Theoretical expressions have been derived for the expected canonical-ensemble specific heat from *KE* fluctuations in microcanonical simulations [11-13]. However, using these expressions for MD simulations at low temperatures (*T*) yield specific heats that are much less than expected from the EFR, as reported previously [14], which can be attributed to excess *KE* fluctuations from the excess *pe* fluctuations that we study here. Anomalously large fluctuations in energy, which increase linearly proportional to the number of particles in the system (*n*), are expected in the theory of small-system thermodynamics (“nanothermodynamics”) [15,16] for the fully-open nanocanonical ensemble due to the unrestricted size of the system [17]. Here we avoid this source of excess fluctuations by studying systems with fixed volume and constrained *n*.

To focus on local energy fluctuations we subdivide large simulations into smaller volumes called “blocks.” Similar subdivisions have long been used for theoretical investigations of fluctuations [18], and

for deriving the canonical and grand-canonical ensembles [19,20]. Early applications to MD simulations of the Lennard-Jones (L-J) model revealed anomalous size-dependent fluctuations in energy and atom density [21,22], but their main focus was to extrapolate to bulk behavior, whereas here we are interested in local effects. Recent studies of the L-J model using the generalized Langevin equation for a central system and its local bath agree with Maxwell-Boltzmann behavior and expected fluctuations [23], but their main focus was on fluctuations in ke . Investigations of small systems at low T have found anomalous fluctuations in both ke and pe [24-26], with various explanations proposed including broken ergodicity, a need to rescale T , and transient normal-modes that become quantum-like at low T . Here we avoid these issues by studying thermal-equilibrium fluctuations about the ground-state energy of small systems ($n=1$ to 6912 atoms) inside much larger simulations that are in the thermodynamic limit, as shown by negligible dependence on the total size of the simulation ($N=55,296$ - $442,368$ atoms). A reduction in pe fluctuations close to the critical point for $n<1000$ has been found in Monte Carlo (MC) simulations of the Ising model for binary “spins” on a lattice [27]. Similar behavior has been attributed to a local thermal bath using nanothermodynamics [28], with reduced fluctuations because the spins have fixed density. Adding a nonlinear correction to Boltzmann’s factor increases the fluctuations, making them consistent with entropy that is extensive and additive. Furthermore, this correction significantly improves agreement between MC simulations of standard models and the measured response of many materials, including critical fluids and ferromagnets [29,30]. Moreover, a related correction provides a common foundation for $1/f$ noise found at low frequencies in most substances [31-33].

Over the past few decades, several fluctuation theorems have been derived for non-equilibrium dynamics [34-40]. Although these theorems should also apply to equilibrium fluctuations, they usually rely on Boltzmann’s factor at some point in the derivation, which requires weak but immediate thermal contact to an effectively infinite heat reservoir [41-44], unlike the behavior found here for the local dynamics of MD simulations. All models we study show significant localization of energy in space, and in time, especially at low temperatures where neighboring atoms move about effectively harmonic pe minima, so that further study will be needed to decide if there is any connection to the localized modes in highly anharmonic lattices [45-47]. Energy localization is also known to occur when phonon wavelengths become comparable to scattering distances in disordered systems [48,49], whereas here we show that energy localization in pure crystals is maximized at lowest temperatures, where disorder is minimized.

Excess energy fluctuations in MD simulations of model crystals may seem similar to measurements of high-purity single crystals at $T<1$ K, where heat capacities can exceed Debye’s theory by an order of magnitude or more [50,51], but various details indicate that there is no clear connection. One detail is that measured heat capacities increase when impurities are added, so that residual deviations from Debye’s theory could come from unavoidable imperfections in even the best crystals available in the laboratory,

while simulations can be done on perfect crystals. More importantly, the experiments measure heat capacity, not energy fluctuations; whereas MD simulations exhibit fundamental deviations from the EFR. Measurements of time-dependent specific heat [52-54] and nonresonant spectral hole burning [55-59] have shown that energy is persistently localized on time-scales of the primary response (e.g. 100 μ s to 100 s) in most types of materials, including liquids, glasses, polymers, and crystals. Other techniques [60-65] have established that this heterogeneity occurs in correlated regions on length-scales of nanometers (e.g. 10 molecules to 390 monomer units [66]), which are uncorrelated with neighboring regions. Although superficially similar to the energy localization we find for MD simulations, various features indicate that there is no clear connection. One feature is that energy localization in measurements persists for times that are several orders of magnitude longer than in the MD simulations, but this may be due to practical limits on the speed of the measurements and the simplicity of the simulated systems. Another feature is that energy localization is most conspicuous in disordered systems; but as in the measurements of low- T heat capacity, increasing disorder may merely increase the magnitude of the effect, with significant energy localization occurring in even the best available crystals. More importantly, various experimental techniques have shown that the localization is associated with abrupt decorrelation across sharp boundaries between neighboring regions in the measurements [67-69], unlike the strong correlations between neighboring blocks in MD simulations. In fact, we suggest that models with interactions that facilitate this decorrelation can improve the agreement between MD simulations, theory, and measured thermal and dynamic properties of materials, as has been done for MC simulations [28-33].

The main conclusion of our study is that excess pe fluctuations occur for all types of small systems inside large simulations, but only if there are long-range interactions. The small systems include individual atoms, and fixed-volume blocks containing 8-6912 atoms, which fluctuate about equilibrium inside much larger simulations that are in the thermodynamic limit, using either pure Newtonian dynamics or a Nosé-Hoover thermostat. Excess pe fluctuations are correlated with atom density, and depend strongly on the interaction cutoff radius. Specifically, pe fluctuations in small systems with long-range interactions exceed the EFR by at least an order of magnitude at low temperatures, dropping abruptly to below the EFR when interactions include only 1st-neighbor atoms. Thus, excess pe fluctuations cannot come from simple surface effects involving robustly harmonic 1st-neighbor interactions, nor from any details in the simulations or analysis. Instead, the mechanism involves the intrinsically anharmonic interactions between 2nd-neighbor atoms, attributable to the local energy reduction when these atoms fluctuate towards the pe minimum at the 1st-neighbor distance. Additional evidence comes from high-frequency normal modes that are found to dominate the excess pe fluctuations, and connect quantitatively to specific zone-boundary phonons that couple primarily to 2nd-neighbor interactions.

II. Background

Standard statistical mechanics is based on Boltzmann's factor, $e^{-E/kT}$, where k is Boltzmann's constant. Boltzmann's factor yields the normalized probability that a given system has energy E , $p_E = e^{-E/kT}/Z$, where Z is the partition function, $Z = \int e^{-E'/kT} g_{E'} dE'$. Here, the density of states often increases as a power-law, $g_E \propto E^\gamma$, with the exponent $\gamma = nD/2 - 1$ for an ideal gas of n atoms moving in D dimensions [19]. The average energy becomes

$$\langle E \rangle = \int E' e^{-E'/kT} g_{E'} dE' / Z. \quad \text{Eq. (1)}$$

According to Feynman [70]: "This fundamental law is the summit of statistical mechanics..." However, Feynman then lists some of the assumptions needed for Eq. (1). "If a system is very weakly coupled to a heat bath at a given 'temperature,' if the coupling is indefinite or not known precisely, if the coupling has been on for a long time, and if all the 'fast' things have happened and all the 'slow' things not, the system is said to be in thermal equilibrium." Thus, three assumptions that may apply to long-time average properties in MD simulations, but not to short-time dynamics, are that the transfer of energy from a local fluctuation to the large reservoir is too slow to control the fast dynamics, so that the dynamics is dominated by a small local bath that interacts strongly with the system, and is altered by the fluctuations so as not to have a unique 'temperature.'

Fluctuation relations connect the internal fluctuations of a thermal quantity to its change with respect to an external parameter [71,72]. Early examples include Einstein's explanation for Brownian motion, which facilitated the first quantitative evidence for atoms [73], and Nyquist's explanation for electron fluctuations that yield Johnson noise [74]. The EFR can be derived from Eq. (1) by taking the

derivative: $\frac{\partial \langle E \rangle}{\partial (kT)} = \frac{\int (E')^2 e^{-E'/kT} g_{E'} dE'}{Z(kT)^2} - \left[\frac{\int E' e^{-E'/kT} g_{E'} dE'}{ZkT} \right]^2 = \frac{\langle E^2 \rangle - \langle E \rangle^2}{(kT)^2}$, yielding:

$$\frac{\partial \langle E \rangle}{\partial (kT)} = \frac{\langle (\Delta E)^2 \rangle}{(kT)^2}. \quad \text{Eq. (2)}$$

Because Eq. (2) is obtained from Eq. (1) using only the product rule of calculus, this EFR is an identity that should apply to any system that exhibits canonical-ensemble dynamics.

Another advantage of the canonical ensemble is that contributions from the kinetic and potential energies are independent. Because the energies add linearly, the left side of Eq. (1) becomes: $\langle KE + PE \rangle = \langle KE \rangle + \langle PE \rangle$. Again taking the derivative of these averages, assuming only the product rule of calculus, Eq. (2) also applies separately to kinetic and potential energies. More generally, from the right side of Eq. (2), $\langle (\Delta KE + \Delta PE)^2 \rangle = \langle (\Delta KE)^2 \rangle + 2\langle \Delta KE \Delta PE \rangle + \langle (\Delta PE)^2 \rangle$, so that the EFR applies separately to KE and PE whenever they fluctuate independently. Indeed, in small blocks at low T we will show that $\langle \Delta KE \Delta PE \rangle \approx 0$, as needed for canonical-ensemble behavior.

The equipartition theorem predicts that average energies have a contribution equal to $\frac{1}{2}kT$ for each classical degree of freedom. The theorem applies to any variable (s) that occurs quadratically in the energy, $E = E_s + E_{(s)}$, where $E_s = \frac{1}{2}Ks^2$ and $E_{(s)}$ is the energy from all variables other than s . Here K is a constant, e.g. the mass of the atom if s is a velocity, or a spring constant if s is a displacement from equilibrium. This theorem can be obtained from Eq. (1) by integrating over all energies using the usual density of states, yielding $\langle E_s \rangle = \frac{\int_0^\infty (E_s')^{\gamma+1} e^{-E_s'/kT} dE_s'}{\int_0^\infty (E_s')^\gamma e^{-E_s'/kT} dE_s'} = kT(\gamma+1) = \frac{1}{2}nDkT$. Thus at low T , where neighboring atoms move in $D=3$ dimensions about a potential-energy minimum that is quadratic, Eq. (2) can be written as:

$$\frac{\partial \langle KE \rangle}{\partial (kT)} + \frac{\partial \langle PE \rangle}{\partial (kT)} = n \frac{3}{2} + n \frac{3}{2} = \frac{\langle (\Delta KE)^2 \rangle}{(kT)^2} + \frac{\langle (\Delta PE)^2 \rangle}{(kT)^2}. \quad \text{Eq. (3)}$$

Theoretically, Eq. (3) is comprised of standard results found in most textbooks on statistical mechanics; empirically, it is the law of Dulong and Petit for measured heat capacities of solids at room temperature. Similar expressions have been derived for energy fluctuations of small systems in the canonical ensemble [75], using nanothermodynamics [17], and an expanded version of thermodynamics [76]. We find that the left-side of Eq. (3) is obeyed by MD simulations, but the right side is not.

III. Simulations

All models were simulated using the Large-scale Atomic/Molecular Massively Parallel Simulator (LAMMPS) [77], with default settings for double precision math and Verlet integration. Here we focus on the standard 12-6 L-J model, with a potential energy that depends on the reduced (dimensionless) distance (r) between interacting atoms, $PE = 4\epsilon \left[\left(\frac{1}{r}\right)^{12} - \left(\frac{1}{r}\right)^6 \right]$, out to a cutoff radius $r < r_c$. For argon the energy scale is set by $\epsilon/k = 119.8$ K while $r=1$ (where $PE=0$) corresponds to 0.3405 nm [78]. A shifted force added to this model (“smooth/linear” option) ensures that both the potential and its derivative go to zero at $r=r_c$. The equilibrium distance between 1st- and 2nd-neighbor atoms is $r_0 \approx 2^{1/6} \approx 1.1225$ and $r_2 \approx 2^{4/6} \approx 1.5874$, respectively. In LAMMPS, potential energy per atom is found by splitting the energy equally between the interacting pair, $pe = PE/2$. This is the simplest way to partition energy between interacting atoms. Furthermore, it yields behavior consistent with energy fluctuations from individual atoms, and from blocks of varying size. The equilibrium structure of the solid phase is a face-centered-cubic (fcc) lattice. Here we focus on two simulation sizes, a cubic volume with sides of length $L=24$ yielding $24^3=13,824$ unit cells containing $N=55,296$ atoms, and $L=48$ yielding $48^3=110,592$ unit cells containing $N=442,368$ atoms. Periodic boundary conditions were used for the outside surfaces in all directions. Many simulations utilized a relatively long cutoff $r_c=6.0$, but crucial information comes from studying how pe fluctuations decrease with decreasing cutoff, at least until there are interactions between only 1st-neighbor atoms, $r_c < r_2 \approx 1.6$. In contrast, because the potential is shifted to equal zero at the cutoff, the average energy per atom at

$kT/\varepsilon=0.001$ increases from $\langle pe \rangle/\varepsilon = -8.461$ for $r_c=6.0$ to -1.535 for $r_c=1.5$. Nevertheless, at such low T the potential well is much deeper than the fluctuations, which even for a single unit cell yields variations in pe of only 0.2-0.4% until $r_c < 1.4$.

We investigate local thermal fluctuations by subdividing the entire simulation volume into smaller cube-shaped “blocks” (chunk/atom compute in LAMMPS), as sketched in Fig. 1. Specific blocks described here have sides of length $\ell=1, 2, 3, 4, 6, 8,$ and 12 unit cells, yielding the number of atoms in equilibrium for the fcc lattice of $\langle n \rangle=4, 32, 108, 256, 864, 2048,$ and 6912 , respectively. (For simulations, angled brackets denote ensemble averages over all equivalent blocks and time averages over the entire production run.) Block positions were usually chosen with walls aligned between crystalline planes, so that most blocks strictly obeyed the canonical ensemble requirement of fixed n . In other simulations the block walls were aligned with the static crystalline planes, facilitating the study of fluctuations in n from even the tiniest motion of the atoms. In this case, canonical ensemble behavior is extracted by averaging the energies only from blocks within a narrow range of atoms, e.g. $n=\langle n \rangle \pm 0.5$, yielding fluctuations in pe and ke that are consistent with fixed n . When blocks are aligned with the crystalline planes, just filling the entire simulation volume, the number of each type ranges between 13,824 blocks for $\ell=1$ in the $L=24$ lattice (or $\ell=2$ in the $L=48$ lattice) to 27 blocks for $\ell=8$ in the $L=24$ lattice (or 64 blocks for $\ell=12$ when $L=48$ lattice). Relatively smooth time-dependent behavior is obtained by averaging over intervals of 10 to 100 time-steps. Several quantities for each block are averaged and recorded after each time interval, including the number of atoms n , potential energy per atom pe , and local temperature from the kinetic energy per atom $kT=2ke/3$. The blocks are purely mathematical, having no influence on the dynamics, so that atoms and energy can transfer freely between blocks, unaffected by block definition. Due to sample symmetry and periodic boundary conditions, each block represents an equivalent central “system,” with neighboring blocks providing a self-consistent bath of energy and atoms, thereby avoiding any issues from artificial thermal baths that may alter intrinsic behavior. Theoretically, such a fixed volume with imaginary walls in a large reservoir of heat and particles is the basis for deriving the grand-canonical ensemble [19], with canonical-ensemble behavior extracted by selecting the subset of blocks with fixed n . Similar fluctuations in energy are found for simulations in the canonical ensemble using the Nosé-Hoover thermostat, and for individual atoms dispersed throughout the system, establishing that the behavior does not depend on block subdivision or energy sharing between atoms or blocks.

Nitromethane (NM) was simulated using interactions and input parameters that are chosen for good agreement with bulk experimental properties as a function of temperature and pressure [79]. The intramolecular potentials come from a superposition of bond-stretching, bond-bending, and torsional-angle terms. The intermolecular potentials include the Buckingham 6-exp form, plus Coulombic interactions. The full simulation volume contains $6 \times 5 \times 4 = 120$ unit cells, for a total of 480 NM molecules ($N=3360$ atoms).

Again local thermal fluctuations are investigated by subdividing into smaller blocks, which are orthorhombic to match the crystalline symmetry. All NM results presented here utilized a single unit cell: $1 \times 1 \times 1$ in the $axbxc$ axis directions, containing 4 molecules, or $\langle n \rangle = 28$ atoms. As with the L-J lattice, each block has a fixed volume and location, filling the entire volume, so that the number of blocks equals the number of unit cells. NM was chosen for study because it provides a system of moderate complexity with realistic potentials, thereby complementing the basic L-J model to establish the generality of the behavior, and because there are other simulations and experiments with which to compare our results.

Production runs for the data presented here were obtained with the full system in the microcanonical ensemble (except for one set of data where the Nosé-Hoover thermostat was added as a test). Thus, the atoms were governed solely by Newton's laws without any additional thermal bath. The equilibrium density of the static crystal was determined by adjusting the density at the lowest T until the lattice had zero pressure ($\rho_0 = 1.09$ for the L-J model), which of course coincides with the minimum pe . To maintain isochoric conditions, some simulations used this same ρ_0 at higher T . Other simulations were initialized using the NPT ensemble to minimize pressure at all T , which yielded similar results throughout the crystalline phase, establishing that thermal expansion does not significantly alter the behavior. The usual time-step was 0.25 fs for NM and 0.001 L-J units for the L-J model, with most production runs lasting 10,000 time-steps. For L-J modeling of Ar [77,78], using $\sqrt{\frac{6.634 \times 10^{-26} \text{ kg}}{\epsilon}} 0.3405 \times 10^{-9} \text{ m} \rightarrow 2.156 \text{ ps}/(\text{L-J unit})$ yields a usual time-step of 2.156 fs. These time-steps were reduced by a factor of 2-10 at higher T , and at lower T to verify that there was negligible integration and averaging error. Indeed the total energy was conserved to within a typical deviation of less than a part per million, with no discernable drift. Similarly there was no discernable drift in the average momentum in each direction. Simulations were initialized for at least 10^5 time-steps before starting the production run. Some simulations were initialized for up to 10^6 time-steps, with no change in the net behavior, confirming that the systems were well-equilibrated. For the L-J model most data were taken during production runs of 200 time intervals (50 time-steps per interval), so that the total number of distinct replicas for each average ranged between 5400 for $\ell = 8$ to more than a million for $\ell = 1$ and 2. For NM, most production runs had 1000 time intervals (10 time-steps per interval) yielding a total of 120,000 distinct replicas. For verification, simulations have been repeated by independent researchers at different laboratories under a wide range of conditions, including different densities, time-step sizes, and time constants for the thermal bath during initialization, always yielding consistent results.

IV. Results

Simulations of the L-J model as a function of the interaction cutoff radius, Fig. 2, establish that 2nd-neighbor interactions are the primary source of excess pe fluctuations. Recall that if $r_c \lesssim 1.6$ interactions are

cutoff before reaching 2nd-neighbor atoms, and that 1st-neighbor interactions are effectively harmonic only if $r_c \gtrsim 1.3$. The solid lines in Fig. 2 show the specific heat from ke (cyan) and pe (purple), which should equal $3/2$ via the equipartition theorem (left side of Eq. (3)). Indeed, from simulations over six temperatures ($kT/\varepsilon=0.0005$ to 0.02) and thirteen cutoff radii ($1.0 \leq r_c \leq 2.5$) the solid cyan line yields $d\langle ke \rangle/d(kT)=1.4992 \pm 0.0007$, while similar averaging of the solid purple line (whenever there is an effectively harmonic interaction, $r_c \geq 1.3$) yields $d\langle pe \rangle/d(kT)=1.494 \pm 0.002$, confirming that these MD simulations give excellent agreement with expected equilibrium average energies. For the dynamics, however, whenever $r_c \geq 1.3$ the normalized energy fluctuations clearly differ from the analogous EFR (right side of Eq. (3)). First focus on the ke fluctuations (red dotted line) that show subtle but significant deviations, $\langle n \rangle \langle (\Delta ke)^2 \rangle / (kT)^2 = 1.356 \pm 0.008$ when averaged over $1.7 \leq r_c \leq 2.5$, with error bars shown from averaging over six temperatures ($kT/\varepsilon=0.0005$ to 0.02). Much more conspicuous are the anomalies in pe fluctuations (open symbols connected by dashed lines), exhibiting distinct regimes of both quantitative and qualitative deviations from the EFR. If there is an effectively harmonic interactions between only 1st-neighbor atoms, $1.3 \leq r_c \leq 1.6$, normalized pe fluctuations are independent of T , but quantitatively the pe fluctuations are about 40% below the specific heat: $\langle n \rangle \langle (\Delta pe)^2 \rangle / (kT)^2 = 0.93 \pm 0.02$ when averaged over six temperatures ($kT/\varepsilon=0.0005$ to 0.02). Whereas, if interactions include 2nd-neighbor atoms $r_c > 1.6$, the normalized pe fluctuations are strongly temperature dependent, diverging as $T \rightarrow 0$. Indeed, energy fluctuations match the specific heat only in the limit of purely repulsive, ideal-gas-like interactions, $r_c < 1.3$. The crucial result established by Fig. 2 is that at low T , pe fluctuations in small blocks are below the expected EFR regardless of the strength of harmonic interaction between 1st-neighbor atoms, with excess pe fluctuations appearing abruptly when the interaction includes more-distant atoms. Thus, these excess pe fluctuations cannot come from any simple interface effect, nor from any artifact in simulating the systems, nor from any procedure in analyzing the results.

Solid symbols and right-hand scale in Fig. 2 present various correlations as a function of r_c . We define the normalized pe correlations between fluctuations in a central block and its η equivalent j^{th} -neighbor blocks by $C_{pe,j}(t) = \eta \frac{\langle \Delta pe_0(0) \Delta pe_j(t) \rangle}{\langle \Delta pe_0(0) \Delta pe_0(0) \rangle}$. (A similar expression gives ke correlations, $C_{ke,j}(t)$.) Here $\eta=1$ when $j=0$ (autocorrelations), while when $j \geq 1$: $\eta=6$ for cubic symmetry in the L-J model (with $\eta=2$ for orthorhombic NM). These values of η ensure that $C_{pe,j}(t)$ includes the total contribution to energy from all equivalent blocks. Specifically, if $1/6$ of the initial pe of an average fluctuation in a cubic block comes from reducing the pe of each 1st-neighbor block, then $C_{pe,1}(0) = 6(-1/6) = -1$ indicates that all of the pe in the fluctuation comes from the six 1st-neighbor blocks, with none of the pe from other blocks, or from ke . Solid squares in Fig. 2 show that the initial ($t=0$) pe correlations between 1st-neighbor blocks ($j=1$) are positive, $C_{pe,1}(0) > 0$, when robustly harmonic interactions occur between only 1st-neighbor atoms

$1.4 \leq r_c \leq 1.6$, coinciding with the reduced pe fluctuations, while $C_{pe,1}(0) < 0$ when interactions include 2nd-neighbor atoms that cause excess pe fluctuations. Solid circles show the normalized cross-correlation between pe and ke within each block, which is significantly negative in the purely harmonic lattice, $C_{kepe,0}(0) = \frac{\langle \Delta ke_0(0) \Delta pe_0(0) \rangle}{\sqrt{\langle (\Delta ke)^2 \rangle \langle (\Delta pe)^2 \rangle}} = -0.047 \pm 0.005$ at $r_c = 1.5$. However, when interactions include 2nd-neighbor atoms ($r_c > 1.6$), $C_{kepe,0}(0) = 0.011 \pm 0.009$ is negligible, as needed for canonical-ensemble behavior. Solid triangles show the normalized cross-correlation between pe and n within each blocks, which is small in the purely harmonic lattice ($r_c \leq 1.6$), $C_{pen,0}(0) = \frac{\langle \Delta pe_0(0) \Delta n_0(0) \rangle}{\sqrt{\langle (\Delta pe)^2 \rangle \langle (\Delta n)^2 \rangle}} = 0.014 \pm 0.003$, but jumps up sharply when $r_c > 1.6$ and reaches 0.506 ± 0.011 for $r_c > 3.0$. Thus, excess pe fluctuations are correlated with n fluctuations and occur only if interactions extend beyond 1st-neighbor atoms, yet such long-range interactions are necessary for the canonical-ensemble requirement of independent fluctuations in ke and pe .

Figure 3 (A) presents the temperature dependence of the ratio of distinct contributions to energy: $\frac{\partial \langle pe \rangle / \partial (kT)}{\partial \langle ke \rangle / \partial (kT)}$ (solid lines) and $\frac{\langle (\Delta pe)^2 \rangle}{\langle (\Delta ke)^2 \rangle}$ (symbols). We use these ratios to remove any artifacts from finite differences in temperature for the derivatives, and finite differences in time for the fluctuations. Red squares and upper scale show NM, other symbols and lower scale show the L-J model. Thus, the L-J data points in Fig. 3 (A) come from the ratio of pe to ke behavior shown in Fig. 2, but as a function of T at fixed values of r_c . For classical particles in the canonical ensemble at low T , pe and ke should give equal contributions to the total energy (left side of Eq. (3)), and its fluctuations (right side of Eq. (3)) [13]. First focus on the solid lines, showing the ratio of temperature derivatives in the LJ model for three different interaction cutoff radii, given by the thickness and color of the line. Deep within the crystalline phase, where each atom oscillates around an effectively harmonic potential in the fcc lattice, the equipartition theorem predicts equal contributions to the specific heat. Indeed, by averaging over five temperatures ($kT/\varepsilon < 0.2$) we find $\frac{\partial \langle pe \rangle / \partial (kT)}{\partial \langle ke \rangle / \partial (kT)} = 0.997 \pm 0.004$, 0.999 ± 0.004 , and 0.9998 ± 0.0013 for $r_c = 1.5$, 2.0, and 6.0, respectively. At higher T , each solid line has a peak that identifies the melting temperature, which ranges from $kT/\varepsilon = 0.75$ to 1.5 for $r_c = 1.5$ to 6.0, consistent with the values of $kT/\varepsilon = 0.78$ to 1.70 found from other simulations at densities of $\rho_0 = 0.97$ to 1.10 [80]. Above the melting temperature each line drops sharply, as expected in the fluid phase where atoms no longer oscillate about a pe minimum. At these high T , the symbols show that the ratio of energy fluctuations also drops sharply $\frac{\langle (\Delta pe)^2 \rangle}{\langle (\Delta ke)^2 \rangle} < 1.0$, consistent with the EFR. However at $kT/\varepsilon \ll 0.1$, symbols show that $\frac{\langle (\Delta pe)^2 \rangle}{\langle (\Delta ke)^2 \rangle} \gg 1.0$ from microcanonical simulations of small blocks $\langle n \rangle = 32$ (circles) and large blocks $\langle n \rangle = 2048$ (solid diamonds) in much larger volumes containing a total number of atoms $N = 55,296$ (open), or $N = 442,368$ (solid), from fluctuations of individual atoms (cyan stars), and from

canonical simulations using the Nosé-Hoover thermostat (open diamonds). Similarly, red squares show that NM has $\frac{\langle(\Delta pe)^2\rangle}{\langle(\Delta ke)^2\rangle} = 3000$ at 0.1 K, and 5.9 at 500 K.

Figure 3 (A) also shows that excess pe fluctuations diverge inversely proportional to temperature at low T . Specifically, $\frac{\langle(\Delta pe)^2\rangle}{\langle(\Delta ke)^2\rangle} = (232 \text{ K})/T$ for NM (red dashed line), while for the L-J model the divergent part of the pe fluctuations can be approximated by the empirical expression $(0.038 \pm 0.003)\epsilon/(kT\ell^{(0.75 \pm 0.05)})$ (black dotted lines). Assuming that this size dependence also applies to much larger simulations, reducing the excess fluctuations to within 10% of the EFR at $kT/\epsilon=0.001$ requires blocks of size $\ell=2750$, corresponding to more than 83 billion atoms. Although uncertainty in the exponent of ℓ allows for the possibility that excess fluctuations could vary as $1/\ell^{0.67}$, the behavior cannot be a simple surface effect in the dominant 1st-neighbor interaction because solid triangles show that the excess pe fluctuations arise abruptly when the cutoff radius is increased to include 2nd-neighbor interactions. Specifically, at low T as r_c increases from 1.5 (down triangles) to 2.0 (up triangles) the ratio $\frac{\langle(\Delta pe)^2\rangle}{\langle(\Delta ke)^2\rangle}$ increases by an order of magnitude due to the onset of the $1/T$ divergence, while the ratio $\frac{\partial\langle pe\rangle/\partial(kT)}{\partial\langle ke\rangle/\partial(kT)}$ is unchanged (solid lines). Thus, although MD simulations accurately yield expected average energies from the left side of Eq. (3), fluctuations show significant deviations from the right side of Eq. (3). Excess pe fluctuations are found for the NM model at most values of T , and in the 12-6 L-J model at low T . To further test our ideas we have found similar excess pe fluctuations in the 9-6 L-J model, reduced pe fluctuations in a lattice of atoms with purely harmonic bonds, and gradual elimination of excess pe fluctuations in the 12-6 L-J model when strong harmonic tethers are added to all atoms, or when a Gaussian potential is added to balance the force between 2nd-neighbor atoms, in general agreement with the interpretations presented here.

Figure 3 (B) shows the initial pe correlations between neighboring blocks. For NM (red squares), this $C_{pe,1}(0)$ reaches -0.96 at 0.1 K. Thus, at 0.1 K, 96% of the pe in a fluctuation of each block ($\langle n \rangle = 28$ atoms) comes from its two neighboring blocks in the a -axis direction. In the L-J model with long-range interactions (black circles, with error bars from averaging over blocks containing $\langle n \rangle = 106$ -2048 atoms), $C_{pe,1}(0)$ varies from 0.067 at high T (black line) to -0.72 at $kT/\epsilon = 0.0005$. Comparison to Fig. 3 (A) reveals that the onset of excess pe fluctuations coincides with the onset of negative $C_{pe,1}(0)$, and that the amplitude of excess pe fluctuations increases monotonically as $C_{pe,1}(0)$ becomes increasingly negative. Similarly for $r_c=2.0$ (up triangles), the onset of excess pe fluctuations in (A) coincides with the onset of negative $C_{pe,1}(0)$ in (B), while for $r_c=1.5$ (down triangles) $C_{pe,1}(0)=0.21 \pm 0.03$ (solid line) shows no tendency towards negative values down to the lowest T . Negative values of $C_{pe,1}(0)$ indicate that an energy increase in the

central block is at least partially compensated by an energy decrease in neighboring blocks, altering the net energy that reaches distant parts of the simulation that serve as the large heat reservoir.

Figures 4 (A)-(C) show the time dependence of pe correlations between blocks containing a single unit cell, from simulations of the L-J model at $kT/\epsilon=0.0005$ (upper two panels) and NM at $T=100$ K. Line color gives the distance between blocks: $j=0$ (black) and $j=1$ (red), with $j=2$ (green) and $j=3$ (blue) in (C) for more-distant blocks. All autocorrelations ($j=0$) approach 1.0 as $t \rightarrow 0$ due to the normalization. For $t > 0$, black and red lines exhibit damped harmonic oscillations that remain roughly 180° out-of-phase in (A) and (C), and roughly in-phase in (B), perpetuating the initial sign of the correlation. Indeed, negative $C_{pe,0}(t) * C_{pe,1}(t)$ for longer-ranged interactions in (A) and (C) indicates that pe is traded back and forth between neighboring blocks, suggesting that short-wavelength motion is involved. In contrast, positive $C_{pe,0}(t) * C_{pe,1}(t)$ for the robustly harmonic lattice in (B) suggests that long-wavelength motion dominates. The green and blue lines in (C) show greatly reduced initial correlations between more-distant blocks. These distant correlations eventually increase with increasing t , then finally decrease, characteristic of a damped wave as excess pe from the fluctuation flows out from the central block. The speed of this wave is obtained from the inset of (C) showing distance to the center of increasingly distant blocks ($j * 0.522$ nm) as a function of time at which each correlation reaches its first maximum. The slope of this line yields 1.11 nm/ps (1110 m/s), somewhat slower than the speed of sound from other simulations (1633 m/s) [81], and from measurements on liquid NM (1300 m/s) [82], which sets the maximum speed of energy dispersal in such insulating substances.

Solid lines in Fig. 4 (D) show the time dependence of ke autocorrelations (black) and correlations between 1st-neighbor blocks (red). In contrast to the corresponding $C_{pe,j}(t)$ in Fig. 4 (C), $C_{ke,j}(t)$ relaxes monotonically, and much slower. Broken lines show fits to the ke autocorrelation: exponential at short times $C_{ke,0}(t) \propto e^{-t/\tau}$ (purple) with a time constant of $\tau=0.41 \pm 0.02$ ps, and stretched-exponential relaxation at longer times $C_{ke,0}(t) \propto e^{-(t/\tau)^\beta}$ (magenta) yielding $\tau=16.5 \pm 0.2$ ps and $\beta=0.73 \pm 0.01$. Previous simulations of NM after excess ke was added to a central molecule find similar timescales, $\tau=11.6$ -13.6 ps, but with $\beta=1$ [83]. The two types of response we find for $C_{ke,0}(t)$ suggest that the short-time behavior comes from localized dynamics, similar to $C_{pe,j}(t)$, while slower relaxation involves transfer of ke to the large heat reservoir, similar to the behavior found in simulations of copper [84]. Measurements of temperature as a function of time after shock-induced ignition in PETN (triangles), and other energetic materials analogous to NM [85], also show a crossover from exponential relaxation at short times to non-exponential relaxation at longer times, somewhat similar to our simulations of $C_{ke,0}(t)$. However, to match the simulations, the measurements were offset by a final temperature and normalized by an initial temperature, with the time

scale reduced by a factor of 100,000. This large difference in time scales could be due to the difference in length scales, or another mechanism, emphasizing the need for further study.

Figure 5 compares frequency-dependent correlations in the energies and density of the L-J model as the interaction cutoff radius is changed from including 2nd-neighbors $r_c = 2.0$ (A) to only 1st-neighbors $r_c = 1.5$ (B). The frequency scale (in THz) is set by the parameters for Ar (2.156 ps/L-J unit). Symbols come from the Fourier transform of normalized autocorrelations in atom density (green triangles), ke (red circles), and pe (black squares), with blue squares from correlations in pe between 1st-neighbor blocks. Fluctuations in n are obtained from simulations having block walls aligned with the equilibrium atomic planes, but other symbols come from separate simulations with blocks shifted to maintain the exact number of atoms $n=108$ (solid) or $n=864$ (open). Data come from averaging spectra at three temperatures ($kT/\varepsilon = 0.0005$ to 0.002, justified at low- T for effectively harmonic modes), with error bars for the solid squares that are visible only if larger than the symbol size. All data are obtained from various correlations as a function of time. For example, the black squares in Figs. 5 (A) and (B) come from the Fourier transform of the respective time-dependent pe autocorrelations, similar to those shown by the black lines in Figs. 4 (A) and (B). Specifically, the pe correlations come from the real part of the discrete Fourier transform, $\sum_{t=-\theta}^{\theta} [C_{pe,j}(|t|)] \cos\left(\frac{2\pi ft}{4\theta}\right)$, with the quantity in square brackets replaced by $C_{ke,0}(|t|)$ or $C_{n,0}(|t|)$ for correlations in ke or n , respectively. For autocorrelations ($j=0$), using the Wiener-Khinchin theorem these yield a power-spectral density, so that separate peaks identify distinct normal modes. Arrows in (A) indicate how various modes in the fluctuations of n and pe shift when the linear size of each block is doubled, $\ell=3 \rightarrow 6$. Key results are found by contrasting the behavior between (A) and (B). First note that only in (A) do pe correlations between 1st-neighbor blocks (blue) show modes that are roughly inverse of the autocorrelations (black), consistent with negative correlations shown in Figs. 2, 3 (B), and 4 that appear abruptly when interactions extend beyond 1st-neighbor atoms. Second, Fig. 5 (B) shows strong similarity between the pe spectra (black squares) and ke spectra (red circles), whereas pe and n (green triangles) are more similar in (A). Finally note that only in (A) do the characteristic frequencies and total number of conspicuous pe modes depend on the size of the block, as indicated by the black arrows. This size dependence from (A) is depicted in the inset of (B), where solid symbols show how various pe modes depend on $1/\ell$. Open symbols in this inset show similar behavior for the n modes, except for the lowest frequency mode that decreases as $1/\ell \rightarrow 0$ (see also the green arrow in (A)), opposite to all pe modes.

Figure 6 shows that for the L-J model at low T , pe and ke fluctuations have starkly different energy distributions when interactions contain distant neighbors, $r_c=6.0$. (Note that pe has been offset by pe_g , the ground-state energy when $T \rightarrow 0$.) The distributions are from histograms for blocks containing a single unit cell, $\langle n \rangle = 4 \pm 0.5$. At low T , pe fluctuations can be characterized by Gaussian distributions (solid lines), indicative of thermal-equilibrium behavior in large systems. At higher T , pe fluctuations are more-

accurately characterized by the canonical-ensemble distribution for small systems [31], $(AE/kT)^\gamma e^{-BE/kT}$ (dashed lines); whereas this distribution holds for the ke fluctuations at all T , indicative of small systems in equilibrium in the canonical ensemble. Here A and B are dimensionless factors that scale the energy E . Expected values are $B=1$ for Boltzmann's factor and $\gamma=3\langle n \rangle/2-1=5$ for an ideal gas. Fits to the ke distributions from the wide range of T in Fig. 6 yield $A=0.237\pm 0.002$ and $B=1.34\pm 0.02$, with $\gamma=7.30\pm 0.06$. Here, $\gamma>5$ indicates that the effective degrees of freedom exceed those expected from the average number of atoms in each block ($n=4\pm 0.5$), attributable to the influence of atoms in neighboring blocks. Indeed, $\gamma=6.06\pm 0.09$ for $n=4\pm 0.0$, while $\gamma\rightarrow 5$ only if the interaction range is reduced to yield 1st-neighbor interactions, $r_c\leq 1.6$ (not shown). In contrast, the pe distributions with long-range interactions have $\gamma\rightarrow\infty$ when $T\rightarrow 0$, where the Gaussian function becomes an excellent approximation to the distributions (solid lines). Thus, with long-range interactions at low T , the effective degrees of freedom for pe fluctuations in each block greatly exceed those of its individual atoms, coinciding with the strong negative correlations between pe in neighboring blocks.

V. Discussion

The simulations presented here show that classical MD simulations of diverse models exhibit energy fluctuations that clearly deviate from standard statistical mechanics. Indeed, Figs. 2 and 3 show that pe fluctuations in nanometer-sized blocks at low T can deviate from the expected EFR by an order of magnitude or more. We now discuss various mechanisms and interpretations that could cause these excess fluctuations.

A) Anomalous pe fluctuations come from localized energy correlations

Figures 2, 3, 4, and 5 establish that excess pe fluctuations inside a central block occur only when there are negative correlations with the pe in the surrounding shell of similar blocks. From Fig. 4 (C) it can be seen that a vanishingly small fraction of the excess pe in a local fluctuation reaches distant blocks before the excess pe returns to zero. Thus, the thermal bath governing pe fluctuations in each system comes primarily from its 1st-neighbor blocks, yielding an explicit local bath that is comparable in size to the system itself; not a large heat reservoir.

The clear connection between energy localization and deviations from the EFR can be characterized by the net energy that reaches the heat reservoir. Specifically, let the PE of the system (central block of n atoms) fluctuate by a total amount $\Delta PE=n\Delta pe$, so that the concurrent change in PE of blocks at distance $j\ell$ is $C_{pe,j}(0)\Delta PE$. For simplicity consider only the dominant correlation from 1st-neighbor blocks, so that the net change for PE fluctuations can be approximated by $(1+C_{pe,1}(0))\Delta PE$, yielding an effective Boltzmann's factor of $e^{-(1+C_{pe,1}(0))\Delta PE/kT}$. Equivalently, the fluctuations can be treated as if each block has an effective

temperature for pe fluctuations of: $T'=T/(1+C_{pe,1}(0))$, where $C_{pe,1}(0)<0$ yields $T'/T>1$. For example, from the black circles and red squares in Fig. 3 (B) at the lowest T , $C_{pe,1}(0) = -0.72$ and -0.96 gives $T'/T=3.6$ and 25 for the L-J model and NM, respectively. In contrast, when the interaction is robustly harmonic between only 1st-neighbor atoms, $C_{pe,1}(0) = +0.21$ (solid line at low T in Fig. 3 (B)) yields a reduced effective temperature, $T'/T=0.83$. Fluctuations from an effective local temperature were used by Einstein in 1910 to describe critical opalescence [86]. More recently, an effective local temperature analogous to our T' has been used to describe the distribution of rings and triplets in amorphous layers of SiO₂ [87], also with $T'/T<1.0$ implying positive correlations, $C_{pe,1}(0)>0$. Another effective temperature can be deduced from the pe fluctuations using the right-side of Eq. (3): $T''/T=\sqrt{\langle(\Delta pe)^2\rangle/\langle(\Delta ke)^2\rangle}$. For $r_c=1.5$, pe fluctuations in the robustly harmonic lattice, $\langle(\Delta pe)^2\rangle/\langle(\Delta ke)^2\rangle=0.651$, yield $T''/T=0.807$, within 3% of the value from pe correlations. Similarly, for $r_c=2.0$ (up triangles) at the lowest T , $C_{pe,1}(0) = -0.5828$ yields $T'/T=2.397$ while $\langle(\Delta pe)^2\rangle/\langle(\Delta ke)^2\rangle=5.700$ yields $T''/T=2.387$. Thus, 1st-neighbor blocks accurately define the effective local temperatures for short-ranged interactions: below the bath T for 1st-neighbor interactions, and above the bath T when 2nd-neighbor interactions are added. Furthermore, for $r_c=6.0$ (black circles and red squares) at the lowest T , $\langle(\Delta pe)^2\rangle/\langle(\Delta ke)^2\rangle=52$ and 3000 gives $T''/T=7.2$ and 55 for the L-J model and NM, respectively. Although these values of T'' are about twice the values of T' , full quantitative agreement is not expected due to additional contributions to T' from more-distant blocks, and from ambiguity in deciding where the local bath ends and the large heat reservoir begins. Nevertheless, the magnitude and sign of pe correlations shown in Fig. 3 (B) control the deviations from the EFR shown in Fig. 3 (A), so that the expected increase or reduction in pe fluctuations can be estimated by knowing the net energy that reaches the large heat reservoir needed for Boltzmann's factor.

Because most models of interacting particles will have correlations that alter the net energy during fluctuations, modifications of Boltzmann's factor may often be necessary to describe the local dynamics. The correction can be approximated by the total energy that reaches the heat reservoir due to direct interactions between the system and surrounding shell of similar systems $\Delta PE \rightarrow (1+C_{pe,1}(0))\Delta PE$, or by an effective local temperature $T'=T/(1+C_{pe,1}(0))$ which is also useful for characterizing local structures [87]. Both interpretations retain the usual Boltzmann's factor for the statistics of fluctuations by simply combining the change in energy of the central block with the change of its shell. A drawback is that $(1+C_{pe,1}(0))\Delta PE$ comes not only from the system, but also from its environment, which must be measured separately or otherwise approximated. An alternate approach that could allow refocusing solely on the system is to include a nonlinear correction from the local entropy. Indeed, a quadratic correction to Boltzmann's factor in the Metropolis algorithm for Monte Carlo simulations alters the pe fluctuations so that they are consistent with entropy that is extensive and additive [28]. Furthermore, this correction

significantly improves agreement between MC simulations of standard models and the measured response of many materials, including critical fluids and ferromagnets [29-33]. Future work will be necessary to determine whether the failure of the EFR for MD simulations may also be treated by a nonlinear correction from the local entropy, without having to include explicit information from surrounding parts of the sample.

B) Excess pe fluctuations come primarily from 2nd-neighbor interactions

Figures 2, 3, and 5 establish that excess pe fluctuations in the L-J model require interactions that extend beyond 1st-neighbor atoms. Thus, a likely mechanism comes from an incipient instability due to the attractive force between 2nd-neighbor atoms. This attractive force tends to favor a type of distortion that can bring 2nd-neighbor atoms closer together, without changing the distance between 1st-neighbors. Specifically, consider three atoms that are initially at the vertices of an isosceles right triangle, somewhat like the symbol Λ , as in the face of an fcc unit cell. Now imagine moving the 2nd-neighbor atoms towards each other to form an equilateral triangle, Δ . If the equilibrium distance between 1st-neighbor atoms is preserved, the net energy of the 2nd-neighbor atoms can be reduced by about 77% (from $-\frac{15}{64}\epsilon$ to $-\epsilon$). Stability against such distortions comes from other atoms in the lattice that maintain the net fcc structure, consistent with the negative correlations in the pe of neighboring blocks as shown in Figs. 2, 3, 4, and 5. Positive correlations between fluctuations in pe and n shown in Figs. 2 and 5 (A) imply that the Δ -like distortion causes additional atoms to move out of the block through the surfaces perpendicular to the axis of the distortion.

Figure 5 reveals several details about the excess pe fluctuations, their connection to atomic motion, and why they are absent if the interaction cutoff is reduced from (A) including 2nd-neighbors $r_c = 2.0$, to (B) only 1st-neighbors $r_c = 1.5$. Fluctuations in n (green triangles) show a large-amplitude low-frequency mode, and multiple mid-frequency modes, all of which simply shift to lower frequencies as r_c is reduced. Fluctuations in ke (red circles) show no mid-frequency modes, but with high-frequency modes that also simply shift to lower frequencies as $r_c = 2.0 \rightarrow 1.5$, again with no obvious change in the general features of the modes. In contrast, pe fluctuations (black squares) are fundamentally altered by the addition of 2nd-neighbor interactions, from closely matching ke fluctuations if $r_c = 1.5$ to matching most of the density modes if $r_c = 2.0$. This abrupt switch in correlation for pe fluctuations from ke to n is confirmed by the switch in Fig. 2 from nonzero solid circles for $r_c \leq 1.6$ to nonzero solid triangles for $r_c > 1.6$. Thus, atomic vibrations that cause the excess pe fluctuations couple strongly to the pe only if the interactions extend beyond 1st-neighbor atoms. As might be expected, atomic motion couples weakly to 1st-neighbor interactions that are robustly harmonic (near the bottom of a potential well), whereas atomic motion couples strongly to 2nd-neighbor interactions that are intrinsically anharmonic (on the side of a potential hill).

C) Excess pe fluctuations involve zone-boundary phonons

Symbols in the inset of Fig. 5 (B) show that all peaks from (A) for both pe (solid) and n (open) vary with the inverse linear dimensions of the block. We use the known dispersion relations of the L-J model (and its similarity to argon) [78,88,89] to assign a specific phonon mode to each peak. The low-frequency mode (found only in the n fluctuations) that initially increases linearly with increasing $1/\ell$ and reaches a maximum at $1/\ell = 0.5$ can be characterized by $f(\text{THz}) = (0.557 \pm 0.008) \sin(\pi/\ell)$ (dashed line). The behavior of this mode is consistent with long-wavelength transverse phonons in the (1,1,1) direction from the Γ - to L-points. pe fluctuations do not couple strongly to this mode because 2nd-neighbor atoms tend to move in-phase for long-wavelength motion, balancing the anharmonic terms. All other modes extrapolate to non-zero frequencies as $1/\ell \rightarrow 0$, characteristic of short-wavelength zone-boundary modes that can be characterized by a quadratic dependence, $f(\text{THz}) = A_i(1/\ell)^2 + C_i$ (solid lines) where A_i is a constant that governs the size dependence of the i^{th} mode, and C_i is its characteristic frequency. We find $C_0 = 1.63 \pm 0.02$, $C_1 = 1.34 \pm 0.04$, $C_2 = 1.10 \pm 0.03$, $C_3 = 0.84 \pm 0.02$, and $C_4 = 0.59 \pm 0.04$, all in THz. The ratio $C_0/C_2 = 1.483$ accurately matches the ratio for longitudinal- to transverse-mode frequencies of 1.480 at the X-point [90]. Although our absolute C_0 is about 12 % below their value of 1.85 THz, the difference can be attributed to different cutoff radii, and their choice of energy and length scales for Ar atoms ($\varepsilon/k = 135$ K and 0.398 nm), which alters the characteristic frequencies. The C_1 frequency is most consistent with the longitudinal mode near the K-point. The C_3 and C_4 frequencies have no clear connection to zone boundary modes. Therefore, we attribute these to transverse phonons with longer wavelengths that nest within larger blocks, consistent with the fact that they do not occur in smaller blocks. Note that the characteristic frequencies of all transverse modes (C_2 - C_4) decrease relatively rapidly with decreasing block size, perhaps because they are governed by shear motion that is softer and more-strongly dependent on the fraction of surface atoms.

D) Theory for excess pe fluctuations

A general theory for excess pe fluctuations comes from considering standard behavior of 1st- and 2nd-neighbor interactions. At sufficiently low- T most 1st-neighbor potentials are robustly harmonic, $pe_1(\delta) \approx \frac{1}{2}a\delta^2$; while the change in energy for each 2nd-neighbor atom yields a potential that is effectively linear, $pe_2(\delta) \approx -b\delta$. Here δ is a relative (dimensionless) displacement, so that constants a and b have units of energy. To be specific, again consider three atoms in the L-J model (fcc lattice) that are initially at the vertices of the isosceles triangle, aligned so that the lower two atoms are on the x -axis, with $r_2 = \sqrt{2}r_0$ the equilibrium (2nd-neighbor) distance between these two atoms, and $r_0 = 2^{1/6}$ the equilibrium (1st-neighbor) distance to the third atom. Assume that only the lower-left atom moves, constrained to stay on the x -axis, with the origin ($x=0$) at the center of its motion. Let the distance between the 2nd-neighbor atoms be reduced to $r_2(1-\delta)$ due to a fluctuation, so that to lowest order the change in their potential is $pe_2(\delta) = \frac{15}{128} \varepsilon +$

$2\varepsilon \left[\left(\frac{1}{r_2(1-\delta)} \right)^{12} - \left(\frac{1}{r_2(1-\delta)} \right)^6 \right] \approx -\varepsilon \frac{21}{32} \delta$. (Note that the potential is divided by 2 to yield the pe of each atom.) The 1st-neighbor atom is at an angle of 45° above the x -axis, so that for small displacements the 1st-neighbor distance becomes $r_0(1-\cos(45^\circ)r_2\delta/r_0) = r_0(1-\delta)$. The lowest-order change in the 1st-neighbor potential is $pe_1(\delta) = \frac{1}{2}\varepsilon + 2\varepsilon \left[\left(\frac{1}{r_0(1-\delta)} \right)^{12} - \left(\frac{1}{r_0(1-\delta)} \right)^6 \right] \approx \frac{1}{2}36\varepsilon\delta^2$. Thus, the total change in pe for the single atom at the origin due to its displacement is: $pe_{1+2}(\delta) = (\frac{1}{2}a\delta^2 - b\delta)$ with $a=36\varepsilon$ and $b=\frac{21}{32}\varepsilon$. Now assume that the quadratic term couples strongly to the thermal bath via harmonic normal modes, while the linear (anharmonic) term is more weakly coupled, e.g. due to Umklapp scattering. Thus, the energy reaching the large thermal reservoir has the same quadratic term, but a different linear term $-c\delta$ (with c constant), so that Boltzmann's factor becomes $g(\delta) = e^{-\frac{1}{2}a\delta^2 - c\delta}/kT$. The average energy is: $\langle pe_{1+2} \rangle = \frac{\int_{-\infty}^{\infty} pe_{1+2}(\delta)g(\delta)d\delta}{\int_{-\infty}^{\infty} g(\delta)d\delta} = \frac{1}{2}kT + \frac{c}{2a}(c - 2b)$, yielding a temperature dependence that is consistent with the left side of Eq. (3) for a single atom ($n=1$) moving in 1-dimension, and an energy reduction for $b > c/2$. Thus, integrating directly over $d\delta$ with $g(\delta)$ (instead of over dE with p_{EGE}) provides an alternative way to derive the equipartition theorem, and the heat capacity is unchanged by linear terms in pe . The analogous fluctuations become $\langle (\Delta pe_{1+2})^2 \rangle = \frac{\int_{-\infty}^{\infty} [pe_{1+2}(\delta)]^2 g(\delta) d\delta}{\int_{-\infty}^{\infty} g(\delta) d\delta} - \langle pe_{1+2} \rangle^2 = \frac{1}{2}(kT)^2 + \frac{(b-c)^2}{a}kT$. Hence, $\frac{\langle (\Delta pe_{1+2})^2 \rangle}{(kT)^2} = \frac{1}{2} + \frac{(b-c)^2}{akT}$ yields a term that agrees with the right side of Eq. (3), plus a term that diverges as $1/T$, qualitatively consistent with the dashed lines in Fig. 3 (A); but only if $c \neq b$. Quantitatively, setting $c=0$ and using $\frac{\langle (\Delta ke)^2 \rangle}{(kT)^2} = \frac{1}{2}$ for motion in one dimension yields $\frac{\langle (\Delta pe_{1+2})^2 \rangle}{\langle (\Delta ke)^2 \rangle} - 1 = \frac{2b^2}{akT} = 0.0239 \frac{\varepsilon}{kT}$, somewhat less than the value of $0.038 \frac{\varepsilon}{kT}$ for $\ell=1$ found in Fig. 3 (A). A better model for the fcc lattice has 12 1st-neighbor atoms yielding $a \rightarrow 12a$, and 6 2nd-neighbors. If these 2nd-neighbor atoms are precisely equidistant from the central atom then $b \rightarrow 0$, valid for static equilibrium and long-wavelength phonons. For local fluctuations, however, a more accurate value comes from the root-mean-squared displacements of the 2nd-neighbor atoms, yielding $b \rightarrow 6 \frac{b}{\sqrt{2}}$ and $\frac{(6b)^2}{12akT} = 0.0359 \frac{\varepsilon}{kT}$, within uncertainty of the $\ell=1$ behavior deduced from Fig. 3 (A). Although this basic model yields behavior consistent with the simulations, a detailed theory must include normal modes for all atoms and interactions, which is a goal for future studies.

Despite its simplicity, the three-atom model exhibits several features found in the simulations. The model shows accurate equipartitioning of the average pe , whereas pe fluctuations diverge proportional to $1/T$, consistent with the dashed lines in Fig. 3 (A). The model often lowers the average pe of the three atoms, at the expense of increased pe from surrounding atoms, consistent with negative correlation of pe in neighboring blocks shown in Figs. 2, 3, 4, and 5. Reduction of pe in the model involves changes in local

density, consistent with the sharp onset of correlations in $\langle pe_0 n_0 \rangle$ when $\langle pe_0 pe_1 \rangle$ becomes negative in Fig. 2, and the similarity in high-frequency modes from pe and n fluctuations shown by the black and green symbols in Fig. 5 (A). Also from Fig. 5 (A) the excess pe fluctuations are coupled to high-frequency zone-boundary modes, consistent with the high-frequency oscillations in pe shown in Figs. 4 (A) and (C). Excess pe fluctuations in the model require anharmonic interactions from the 2nd-neighbor atom, consistent with the sharp onset of excess pe fluctuations and negative correlations in $\langle pe_0 pe_1 \rangle$ that coincide with the onset of 2nd-neighbor interactions shown in Fig. 2. Thus, Δ -like distortions that transiently reduce the local pe are the likely cause of excess pe fluctuations in the simulations. Indeed, using Ovito visualization software [91] to analyze atom positions of the L-J model reveals that there is a small but significant increase in the relative variance of 2nd-neighbor distances with the onset of 2nd-neighbor interactions, $1.023 \rightarrow 1.044 \pm 0.003$. No such increase in variance is found for the distances to other neighbors, confirming that 2nd-neighbor interactions dominate the excess pe fluctuations in the simulations. Finally, excess pe fluctuations in the model require that the local pe differs from the energy used in Boltzmann's factor, $c \neq b$. This requirement is consistent with the effective local temperature used to describe the simulations, as well as the strong negative correlations between 1st-neighbor blocks shown in Figs. 2, 3, 4, and 5 (A), and the finite speed of the energy flow shown in the inset of Fig. 4 (C), establishing that local changes in pe do not immediately reach the large heat reservoir needed for Boltzmann's factor.

E) Heterogeneity as a mechanism for thermal dynamics in MD simulations

Figure 6 shows very broad pe distributions at low T , often with $pe < pe_g$ from blocks having multiple atoms below their ground-state energy, consistent with an incipient Δ -like distortion that lowers the local energy. For example at $kT/\varepsilon = 0.001$, 39% of the blocks have $pe < pe_g$. Net reduction in pe is inhibited by the increased energy of the surrounding sample, consistent with the negative correlation between neighboring blocks shown in Figs. 2, 3, 4, and 5. Thus, any mechanism that decorrelates neighboring blocks would reduce the net pe of each block, as found for MC simulations [28-33]. Many experimental techniques have shown that most materials have a mechanism that decorrelates neighboring regions [60-69], unlike the uniform correlations in MD simulations of homogeneous models. These nanometer-sized regions form an ensemble of independent small system, which must be treated using the theory of small system thermodynamics [16]. This nanothermodynamics provides the theoretical foundation for treating small systems in thermal contact with an ensemble of similarly small systems [15]. Moreover, a heterogeneous distribution of independently relaxing regions provides a basic mechanism for coarse graining in the dynamics, which was already recognized by Gibbs as a way to connect reversible Newtonian mechanics with irreversible thermodynamics [92]. We anticipate that adding heterogeneity to MD simulations via a

mechanism that decorrelates neighboring blocks will improve agreement with measurements, and with nanothermodynamics, as has been found for MC simulations [28-33].

VI. Conclusions

We extend the original goal of Enrico Fermi and his team to compare equilibrium MD simulations based on Newton's laws with standard statistical mechanics based on Boltzmann's factor. We find that the average energies give excellent agreement with the equipartition theorem, but energy fluctuations deviate significantly from the analogous energy fluctuation relation, especially at low temperatures. In fact, excess pe fluctuations tend to diverge inversely proportional to T , as shown in Fig. 3 (A). Empirically, at the lowest T studied, pe fluctuations can be characterized by an effective temperature that is an order of magnitude hotter than the temperature for ke fluctuations. These deviations occur in thermal equilibrium for fluctuations of individual atoms, as well as for blocks containing 8-6912 atoms inside much larger simulations that are in the thermodynamic limit, using either pure Newtonian dynamics or a Nosé-Hoover thermostat. Figure 2 establishes that abruptly when the interaction cutoff radius is reduced to include only the robustly harmonic interaction between 1st-neighbor atoms, the pe fluctuations are reduced below the ke fluctuations. Thus, excess pe fluctuations require long-ranged interactions, and are not an artifact from simple interface effects in the strongest interaction, nor from details in the simulations or data analysis.

We elucidate the source of anomalous fluctuations using energy correlations as a function of time and distance. Figures 2 and 3 show a clear connection between the excess pe fluctuations in small blocks and negative correlations in the pe between neighboring blocks, whereas for reduced pe fluctuations this correlation is positive. Figures 3 and 4 confirm that anomalous pe fluctuations in small blocks involve energy that is localized to a surrounding shell of similarly small blocks. Figure 4 (C) also shows that Δpe oscillates rapidly, passing through zero before the speed of sound carries excess pe much beyond the neighboring blocks, isolating the local dynamics from the large heat reservoir needed to justify Boltzmann's factor. Combining the PE of each block with the PE of its neighboring blocks yields a modified energy for Boltzmann's factor, or equivalently an effective local temperature that often agrees quantitatively with the one deduced from anomalous pe fluctuations. Figure 2 shows that excess pe fluctuations become reduced pe fluctuations abruptly when the interaction cutoff is reduced to yield interactions only between 1st-neighbor atoms. Figures 2 and 5 show that excess pe fluctuations are connected to density fluctuations, but only if there are 2nd-neighbor interactions. We attribute the mechanism to an incipient local distortion that transiently brings 2nd-neighbor atoms closer to their lower-energy 1st-neighbor distance, which can significantly lower the interaction energy in localized regions, but yields high-energy boundaries between these regions. Figure 6 shows the resulting increased width in the pe distribution at low T . A basic model is presented that quantitatively characterizes various features in the simulations. A crucial ingredient in the

model is that Boltzmann's factor must be modified to eliminate (or at least reduce) the pe from 2nd-neighbor atoms. The mechanism is attributable to the fact that intrinsically anharmonic interactions between 2nd-neighbor atoms do not couple strongly to long-wavelength normal modes, becoming isolated from the large heat reservoir due to anharmonic processes such as Umklapp scattering. In other words, the 2nd-neighbor interactions that dominate the excess pe fluctuations are disconnected from Boltzmann's factor, consistent with the localized energy that we find from pe correlations. Because most models of practical importance include interactions that are not robustly harmonic, similar excess pe fluctuations are expected in most MD simulations.

We know of no unambiguous experimental evidence for the excess pe fluctuations that we find in MD simulations. Insight comes from the excess specific heat found in most substances at low temperatures [50-52,54]. Indeed, high-purity single crystals at $T < 1$ K exhibit excess specific heat that diverges from Debye's theory inversely proportional to a power of T , superficially similar to the $1/T$ divergence of excess pe fluctuations in the simulations. Furthermore, amorphous materials have much stronger deviations from Debye's theory, as expected when disorder causes many 1st-neighbor atoms to deviate from their robustly harmonic pe minimum. Thus, the 2-level system behavior that is well-known in amorphous materials could come from anharmonic interactions that are weakly coupled to the thermal bath at low T . Although we emphasize that the simulations show excess pe fluctuations, not excess specific heat, a connection could occur if the energy fluctuation relation violated in MD simulations is at least partially restored in real materials. The mechanism likely involves quantum effects, such as those that are necessary for correct behavior of the specific heat below the Debye temperature, which is an area for future investigation.

Our study reveals a fundamental inconsistency in the dynamics deduced from classical MD simulations, theory, and experiments. Specifically, we have shown that excess pe fluctuations from MD simulations based on Newton's laws often differ significantly from standard statistical mechanics based on Boltzmann's factor; and that neither approach fully explains the thermodynamic heterogeneity and excess specific heat found by several experimental techniques in disordered materials and high-purity single crystals, especially at low temperatures [50-69]. Our MD simulations and analysis show that anomalous pe fluctuations in nanometer-sized subsystems come from temporal memory effects and spatial correlations in the surrounding shell of similarly small systems, which are effectively isolated from the large heat reservoir needed for Boltzmann's factor. Prior progress in the theoretical understanding of small systems has been made by adding thermodynamic heterogeneity to statistical mechanics using nanothermodynamics as a guide [15], yielding a nonlinear correction to Boltzmann's factor that facilitates the self-consistent treatment of small systems in thermal contact with an ensemble of similarly small systems [16]. For MD simulations we expect that adding thermodynamic heterogeneity will reduce high-energy boundaries between neighboring regions, lower the total energy at a given temperature, and restore energy fluctuation relations

for the dynamics. The requisite mechanism must yield independent fluctuations for the potential energy from neighboring regions, possibly from quantum-correlation effects for the behavior of atoms on the scale of nanometers [93]. Specifically for the L-J model, heterogeneity could arise from the van der Waals ($1/r^6$) interaction, which involves coherent fluctuations between induced dipoles. Maintaining this coherence within nanometer-sized regions, while breaking the coherence between neighboring regions, would yield thermodynamic heterogeneity found in experiments, and reduce the negative correlations that cause excess pe fluctuations in MD simulations. A similar decorrelation between nanometer-sized regions in MC simulations has been achieved using a nonlinear correction to the Metropolis algorithm, which significantly improves agreement between standard models and measured behavior [28-33]. We anticipate that adding thermodynamic heterogeneity to models and/or algorithms in MD simulations will decorrelate the dynamics between local region in the simulations, allowing access to lower-energy states and reduced pe fluctuations, while providing an intrinsic mechanism for coarse graining. Such thermodynamic heterogeneity should also improve agreement between MD simulations, theoretical fluctuation relations, and measured behavior.

VII. Acknowledgments

We are grateful for helpful discussions with S. Abe, O. Beckstein, B. F. Davis, J. Dyre, K. Ghosh, A. Heuer, M. Heyden, Y. Li, N. Newman, J. B. Page, B. M. Rice, S. L. Seyler, and G. H. Wolf. RVC has the pleasure to thank Betsy Rice and her team for their hospitality and assistance during a stay at the Army Research Laboratory. Most of the simulations were performed using the facilities of ASU Research Computing.

References

- ¹ E. Fermi, J. R. Pasta, and S. Ulam, *Report LA-1940*. Los Alamos Scientific Laboratory (1955).
- ² W. G. Hoover, *Time reversibility, computer simulations, and chaos* (World Scientific, Singapore, 1999).
- ³ N. Komatsu and T. Abe, *Computer Phys. Comm.* **171**, 187 (2005).
- ⁴ R. H. Swendsen, *Am. J. Phys.* **76**, 643 (2008).
- ⁵ M. A. Porter, N. J. Zabusky, B. Hu, and D. K. Campbell, *American Scientist* **97**, 214 (2009).
- ⁶ G. P. Berman and F. M. Izrailev, *Chaos* **15**, 015104 (2005).
- ⁷ A. Carati and L. Galgani, *Europhys. Lett.* **75**, 528 (2006).
- ⁸ H. J. Matsuyama and T. Konishi, *Phys. Rev. E* **92**, 022917 (2015).
- ⁹ C. Danieli, D. K. Campbell and S. Flach, *Phys. Rev. E* **95**, 060202 (2017).
- ¹⁰ R. Kashyap, A. Westley, A. Datta and S. Sen, *Int. J. Mod. Phys. B* **31**, 1742014 (2017).
- ¹¹ J. L. Lebowitz, J. K. Percus and L. Verlet, *Phys. Rev.* **153**, 250 (1967).
- ¹² E. M. Pearson, T. Halicioglu and W. A. Tiller, *Phys. Rev. A* **32**, 3030 (1985).
- ¹³ M. P. Allen and D. J. Tildesley, *Computer Simulation of Liquids* (Oxford University Press, 1987).
- ¹⁴ A. Perronace and A. Tenenbaum, *Phys. Rev. E* **57**, 100 (1998).
- ¹⁵ T. L. Hill, *Thermodynamics of small systems (Parts I and II)*, (Dover, Mineola, NY, 1994).
- ¹⁶ R. V. Chamberlin, *Entropy* **17**, 52 (2015).
- ¹⁷ T. L. Hill and R. V. Chamberlin, *Nano Lett.* **2**, 609 (2002).
- ¹⁸ M. J. Klein and L. Tisza, *Phys. Rev.* **76**, 1861 (1949).
- ¹⁹ T. L. Hill, *An Introduction to Statistical Thermodynamics*, (Dover, Mineola, NY, 1986).
- ²⁰ R. K. Pathria and P. D. Beale, *Statistical Mechanics 3rd Ed.* (Butterworth-Heinemann, Oxford, 2011).
- ²¹ M. Rovere, D. W. Hermann, and K. Binder, *Europhys. Lett.* **6**, 585 (1988).
- ²² M. Rovere, P. Nielaba, and K. Binder, *Z. Phys. B* **90**, 215 (1993).
- ²³ H. Ness, L. Stella, C. D. Lorenz, and L. Kantorovich, *Phys. Rev. B* **91**, 014301 (2015).

-
- ²⁴ U. A. Salian, *J. Chem. Phys.* **108**, 6342 (1998).
- ²⁵ R. Simonazzi and A. Tenenbaum, *Phys. Rev. E* **54**, 964 (1996).
- ²⁶ G. Marcelli and A. Tenenbaum, *Phys. Rev. E* **68**, 041112 (2003).
- ²⁷ K. Binder, *Z. Phys. B* **43**, 119 (1981).
- ²⁸ R. V. Chamberlin and G. H. Wolf, *Eur. Phys. J. B* **67**, 495 (2009).
- ²⁹ R. V. Chamberlin, J. V. Vermaas, and G. H. Wolf, *Eur. Phys. J. B* **71**, 1 (2009).
- ³⁰ R. V. Chamberlin, *Physica A* **391**, 5384 (2012).
- ³¹ R. V. Chamberlin and D. M. Nasir, *Phys. Rev. E* **90**, 012142 (2014).
- ³² R. V. Chamberlin, S. Abe, B. F. Davis, P. E. Greenwood, and A. S. H. Shevchuk, *Eur. Phys. J. B* **89**, 185 (2016).
- ³³ R. V. Chamberlin, *Eur. Phys. J. Special Topics* **226**, 365 (2017).
- ³⁴ D. J. Evans, E. G. D. Cohen, and G. P. Morriss, *Phys. Rev. Lett.* **71**, 2401 (1993).
- ³⁵ G. Gallavotti and E. G. D. Cohen, *Phys. Rev. Lett.* **74**, 2694 (1995).
- ³⁶ C. Jarzynski, *Phys. Rev. Lett.* **78**, 2690 (1997).
- ³⁷ G. E. Crooks, *Phys. Rev. E* **60**, 2721 (1999).
- ³⁸ R. Kawai, J. M. R. Parrondo, and C. Van den Broek, *Phys. Rev. Lett.* **98**, 080602 (2007).
- ³⁹ S. Pressé, K. Ghosh, J. Lee, and K. A. Dill, *Rev. Mod. Phys.* **85**, 1115 (2013).
- ⁴⁰ U. Seifert, *Rep. Prog. Phys.* **75**, 1 (2012).
- ⁴¹ J. L. Lebowitz and H. Spohn, *J. Stat. Phys.* **95**, 333 (1999).
- ⁴² E. G. D. Cohen and D. Mauzerall, *J. Stat. Mech: Theor. Exp.* P07006 (2004).
- ⁴³ C. Jarzynski, *J. Stat. Mech: Theor. Exp.* P09005 (2004).
- ⁴⁴ M. Cuendet, *J. Chem. Phys.* **125**, 144109 (2006).
- ⁴⁵ A. J. Sievers and S. Takeno, *Phys. Rev. Lett.* **61**, 970 (1988).
- ⁴⁶ J. B. Page, *Phys. Rev. B* **41**, 7835 (1990).
- ⁴⁷ S. Flach and A. V. Gorbach, *Phys. Rep.* **467**, 1 (2008).

-
- ⁴⁸ P. W. Anderson, *Phys. Rev.* **109**, 1492 (1958).
- ⁴⁹ A. Lagendijk, B. van Tiggelen, and D. S. Wiersma, *Phys. Today* **62**, 24 (2009).
- ⁵⁰ D. A. Ackerman, D. Moy, R. C. Potter, A. C. Anderson, and W. N. Lawless, *Phys. Rev. Lett.* **23**, 3886 (1981).
- ⁵¹ W. Knaak and M. Meissner, pgs. 416-418 in *Phonon Scattering in Condensed Matter* (Springer-Verlag, Berlin, 1984).
- ⁵² M. Meissner and K. Spitzmann, *Phys. Rev. Lett.* **46**, 265 (1981).
- ⁵³ P. K. Dixon and S. R. Nagel, *Phys. Rev. Lett.* **61**, 341 (1988).
- ⁵⁴ N. Sampat and M. Meissner, pgs. 105-112 in: *Die Kunst of Phonons*, ed. by T. Paszkiewicz and K. Rapcewicz (Springer, Boston, 1994).
- ⁵⁵ B. Schiener, R. Böhmer, A. Loidl, and R. V. Chamberlin, *Science* **274**, 752 (1996).
- ⁵⁶ R. V. Chamberlin, *Phase Transitions* **65**, 169 (1998).
- ⁵⁷ R. V. Chamberlin, *Phys. Rev. Lett.* **83**, 5134 (1999).
- ⁵⁸ R. Richert and S. Weinstein, *Phys. Rev. Lett.* **97**, 095703 (2006).
- ⁵⁹ R. V. Chamberlin, R. Böhmer, and R. Richert, pgs. 127-185 in: *Nonlinear dielectric spectroscopy*, ed. by R. Richert, (Springer, Cham, Switzerland, 2018).
- ⁶⁰ E. Donth, *J. Non-Cryst. Solids* **53**, 325 (1982).
- ⁶¹ V. I. Yukalov, *Phys. Rep.* **208**, 395 (1991).
- ⁶² R. Böhmer, R. V. Chamberlin, G. Diezemann, B. Geil, A. Heuer, G. Hinze, S. C. Kuebler, R. Richert, B. Schiener, H. Sillescu, H. W. Spiess, U. Tracht, and M. Wilhelm, *J. Non-Cryst. Solids* **235-237**, 1 (1998)
- ⁶³ M. D. Ediger, *Annu. Rev. Phys. Chem.* **51**, 99 (2000).
- ⁶⁴ R. Richert, *J. Phys. Condens. Matter* **14**, R703 (2002).
- ⁶⁵ L. J. Kaufman, *Ann. Rev. Phys. Chem.* **64**, 177 (2013).
- ⁶⁶ S. A. Reinsberg, A. Heuer, B. Doliwa, H. Zimmermann, H. W. Spiess, *J. Non-Cryst. Sol.* **307-310**, 208 (2002).
- ⁶⁷ U. Tracht, M. Wilhelm, A. Heuer, H. Feng, K. Schmidt-Rohr, and H. W. Spiess, *Phys. Rev. Lett.* **81**, 2727 (1998).
- ⁶⁸ X. Qiu, T. Proffen, J. F. Mitchell, and S. J. L. Billing, *Phys. Rev. Lett.* **94**, 1772033 (2005).

-
- ⁶⁹ W. Huang and R. Richert, *J. Chem. Phys.* **130**, 194509 (2009).
- ⁷⁰ R. P. Feynman, *Statistical Mechanics: A set of lectures*, Chapter 1 (Westview Press, Boulder, CO, 1998).
- ⁷¹ R. Kubo, *Rep. Prog. Phys.* **29**, 255 (1966).
- ⁷² U. M. B. Marconi, A. Puglisi, L. Rondoni, and A. Vulpiani, *Phys. Rep.* **461**, 111 (2008).
- ⁷³ R. Newburgh, J. Peidle, and W. Rueckner, *Am. J. Physics* **74**, 478 (2006).
- ⁷⁴ J. G. Hoffman, *Phys. Today* **15**, 30 (1962).
- ⁷⁵ H. B. Callen, *Thermodynamics and an introduction to thermostatistics*, 2nd ed. Chapter 16 (Wiley, New York, NY, 1985).
- ⁷⁶ Y. Mishin, *Ann. Phys.* **363**, 48 (2015).
- ⁷⁷ S. Plimpton, *J. Comp. Phys.* **117**, 1 (1995); <https://lammps.sandia.gov/doc/Manual.html>
- ⁷⁸ J. A. White, *J. Chem. Phys.* **111**, 9352 (1999).
- ⁷⁹ D. C. Sorescu, B. M. Rice, D. L. Thompson, *J. Phys. Chem. B* **104**, 8406 (2000).
- ⁸⁰ E. A. Mastny and J. J. de Pablo, *J. Chem. Phys.* **127**, 104504 (2007).
- ⁸¹ M. Zhong, Q. J. Liu, H. Qin, Z. Jiao, F. Zhao, H. L. Shang, F. S. Liu and Z. T. Liu, *Eur. Phys. J. B* **90**, 115 (2017).
- ⁸² B. O. Reese, L. B. Seely, R. Shaw and D. Tegg, *J. Chem. Eng. Data* **15**, 140 (1970).
- ⁸³ L. A. Rivera-Rivera, A. Siavosh-Haghighi, T. D. Sewell, and D. L. Thompson, *Chem. Phys. Lett.* **608**, 120 (2014).
- ⁸⁴ J. Hickman and Y. Mishin, *Phys. Rev. B* **94**, 184311 (2016).
- ⁸⁵ W. P. Bassett, B. P. Johnson, N. K. Neelakantan, K. S. Suslick, and D. D. Dlott, *Appl. Phys. Lett.* **111**, 061902 (2017).
- ⁸⁶ A. Einstein, *Ann. der Phys.* **33**, 1275 (1910).
- ⁸⁷ P. K. Roy and A. Heuer, <https://arxiv.org/abs/1808.03869>
- ⁸⁸ V. V. Goldman, G. K. Horton, T. H. Keil and M. L. Klein, *J. Phys. C: Solid State Phys.* **3**, L33 (1970).
- ⁸⁹ Y. Fujii, N. A. Luris, R. Pynn and G. Shirane, *Phys. Phys. B* **10**, 3647 (1974).
- ⁹⁰ P. T. Jochym, M. Sternik and K. Parliński, *Comp. Mat. Sci.* **6**, 339 (1996).

⁹¹ A. Stukowski, *Modelling Simul. Mat. Sci. Eng.* **10**, 015012 (2010); <http://ovito.org/>.

⁹² J. L. Lebowitz, *Physica A* **194**, 1 (1993).

⁹³ L. Brus, *Accts. Chem. Res.* **47**, 2951 (2014).

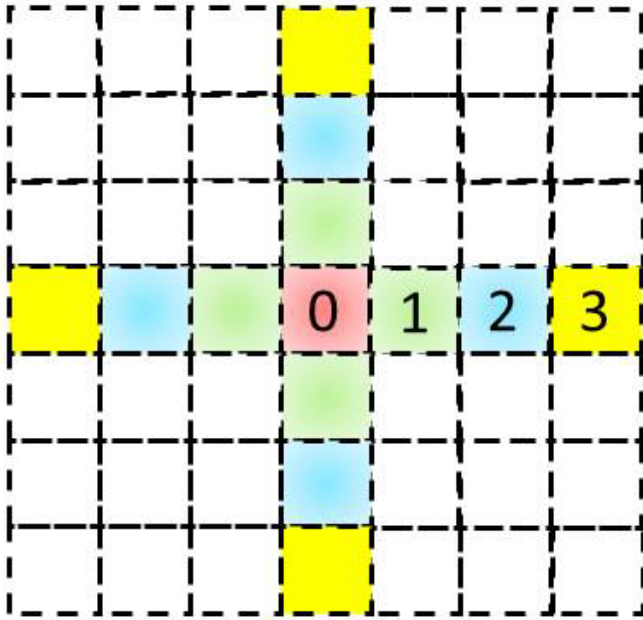


FIG. 1. (Color online) Schematic representation of small blocks that form local systems inside a much larger simulation volume. Each block encompasses an integer number of unit cells, so they are cube-shaped for the L-J model and orthorhombic for NM. A central block is labeled “0”, a 1st-neighbor block is labeled “1”, etc. Periodic boundary conditions are used on all outside surfaces, so that optimal statistics is achieved using ensemble-averaging with each block as the center “0,” and time-averaging over the entire production run for equilibrium behavior. Similarly, time-dependent properties are deduced from ensemble averaging the behavior of individual blocks at times separated by t , averaged over the entire production run. Each block mimics the textbook example of a system that is in the grand-canonical ensemble. Canonical-ensemble behavior is extracted by selecting the subset of blocks that have the equilibrium number of atoms in each block.

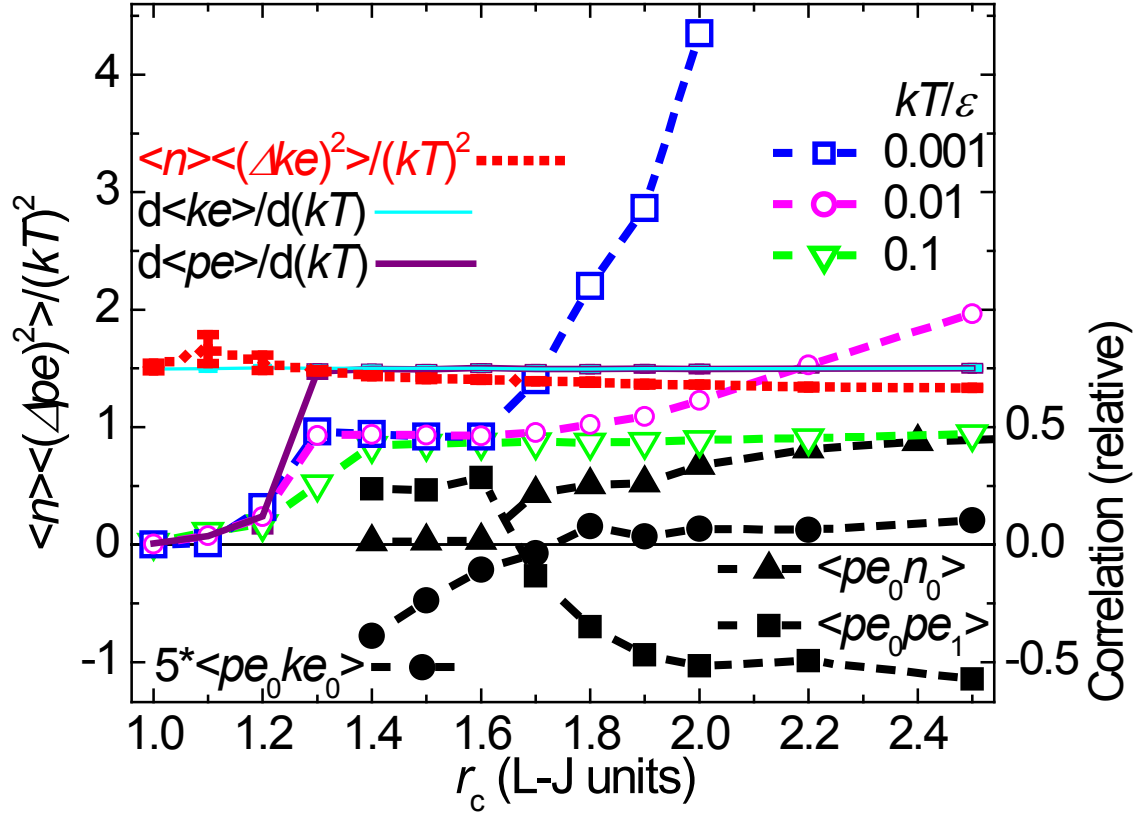


FIG. 2. (Color online) Interaction cutoff radius dependence of normalized energy fluctuations and specific heat (left scale), and correlations (right scale), from blocks having $n=32$ in the L-J model. Note that for $r_c \leq 1.6$ the only interaction is between 1st-neighbor atoms, which is robustly harmonic at low T for $r_c \geq 1.3$. Open symbols show fluctuations in pe at three T (given in the legend), with dashed lines connecting the symbols as a guide for the eye. The dotted red line shows analogous fluctuations in ke , with error bars from averaging over six T ($kT/\epsilon=0.0005$ to 0.02). Solid lines show the T -dependent derivatives of $\langle ke \rangle$ (cyan) and $\langle pe \rangle$ (purple), averaged over the same range of T , with error bars visible due to the line thickness. Solid symbols (from simulations at $kT/\epsilon=0.001$) show normalized correlations of pe in each central block with ke (circles), with n (triangles), as well as with pe in neighboring blocks (squares). The EFR predicts identical values for the dotted red and solid cyan lines, as well as for the open symbols and solid purple line, found only for short-ranged purely repulsive forces, $r_c < 1.3$. Note that in general, positive $\langle pe_0 pe_1 \rangle$ yields pe fluctuations that are significantly below the EFR, whereas negative $\langle pe_0 pe_1 \rangle$ when $r_c > 1.6$ yields excess pe fluctuations that diverge with decreasing T .

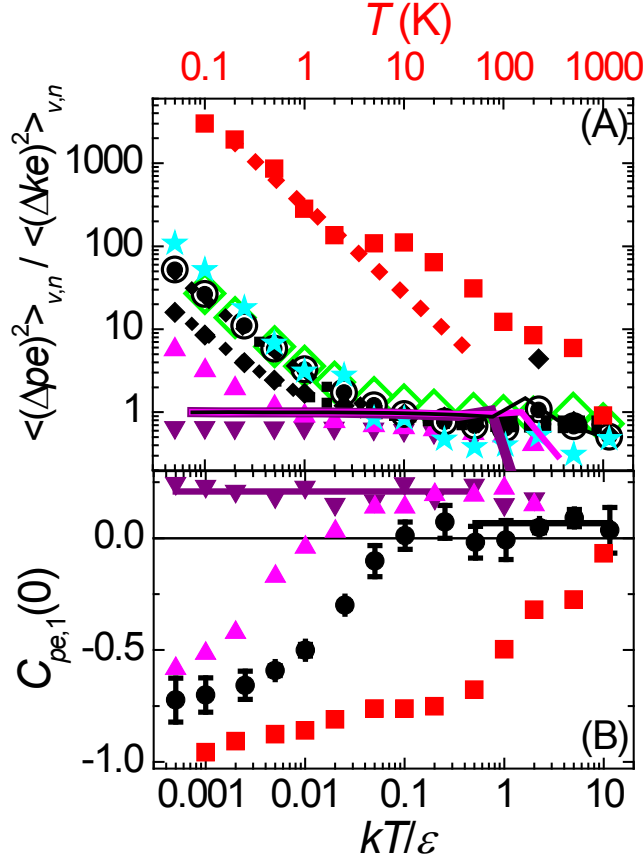


FIG. 3 (Color online) (A) Symbols show the ratio of local energy fluctuations, from simulations of NM (squares) with T in K (top scale), and the L-J model (other symbols) with T in L-J units (bottom scale). These T were calculated from the kinetic energy per atom, averaged over all blocks with the correct $\langle n \rangle$. Open circles are from blocks containing $\langle n \rangle = 32$ atoms inside simulations containing $N = 55,296$ atoms, solid symbols are from blocks with $\langle n \rangle = 32$ (circles) and $\langle n \rangle = 2048$ (diamonds) with $N = 442,368$, while stars come from individual atoms. Open diamonds show simulations using a Nosé-Hoover thermostat, while all other simulations use pure Newtonian dynamics. Dotted lines show the $1/T$ divergence of excess pe fluctuations as $T \rightarrow 0$. Triangles show analogous simulations to the solid circles, except that the interaction range is reduced to include only 1st-neighbor atoms $r_c = 1.5$ (down), or also 2nd-neighbor atoms $r_c = 2.0$ (up). Solid lines that vary from thick to thin show the ratio of average specific heats, $\frac{\partial \langle pe \rangle / \partial (kT)}{\partial \langle ke \rangle / \partial (kT)}$, for interaction cutoff radii in the L-J model of $r_c = 1.5, 2.0,$ and 6.0 , with peaks that identify the melting temperatures of $kT/\epsilon = 0.75, 1.5,$ and 1.5 , respectively. (B) Initial pe correlations between 1st-neighbor blocks in the L-J model with $r_c = 1.5$ (down triangles), 2.0 (up triangles), and 6.0 (circles), and in NM (squares). Solid lines show average values where the behavior is independent of T . Down triangles in (A) and (B) show that $r_c = 1.5$ yields fluctuations below the EFR prediction, with positive initial correlations, opposite to the low- T behavior of analogous simulations with long-range interactions (other symbols).

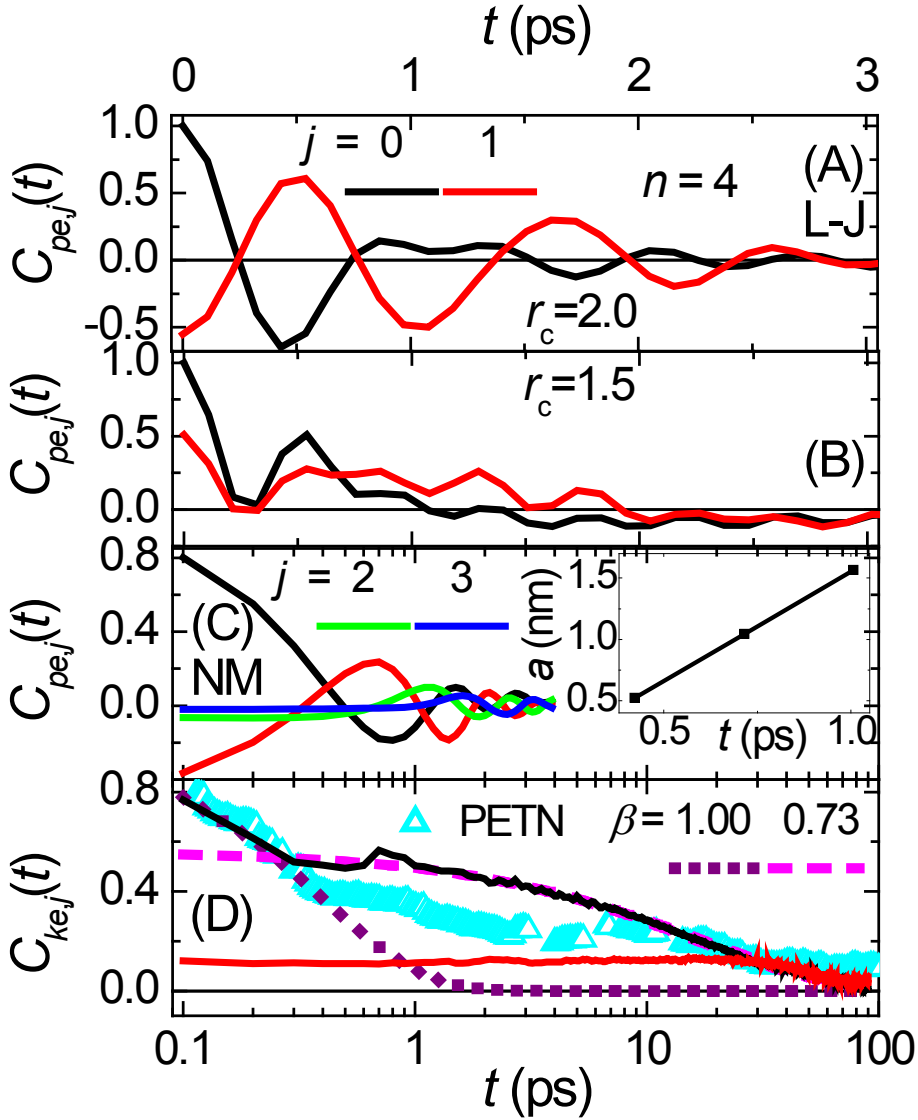


FIG. 4. (Color online) Upper two panels show time-dependent pe autocorrelations (black) and correlations between 1st-neighbor blocks (red), with time on a linear scale (upper axis) using 2.156 ps/(L-J unit). These upper panels are from the L-J model at $kT/\epsilon=0.0005$ in blocks having $n=4$ with cutoff radii of 2.0 (A) and 1.5 (B). Lower two panels show correlations in pe (C) and ke (D), from the a -axis of NM at $T=100$ K, with time on a logarithmic scale (lower axis). (C) also shows pe correlations to more-distant blocks: $j=2$ (green) and $j=3$ (blue). The inset of (C) shows the distance between 1st-, 2nd-, and 3rd-neighbor blocks as a function of time at which the pe correlations reach their first maximum, which yields the solid line of slope 1.11 nm/ps (1110 m/s). Broken lines in (D) are from fits to the ke autocorrelation showing exponential relaxation at short times (dotted) and stretched-exponential at long times (dashed). Triangles in (D) show temperature as a function of time from measurements of PETN [85], with the x - and y -axes offset and/or multiplied by a factor to put them on the same scale as the simulations.

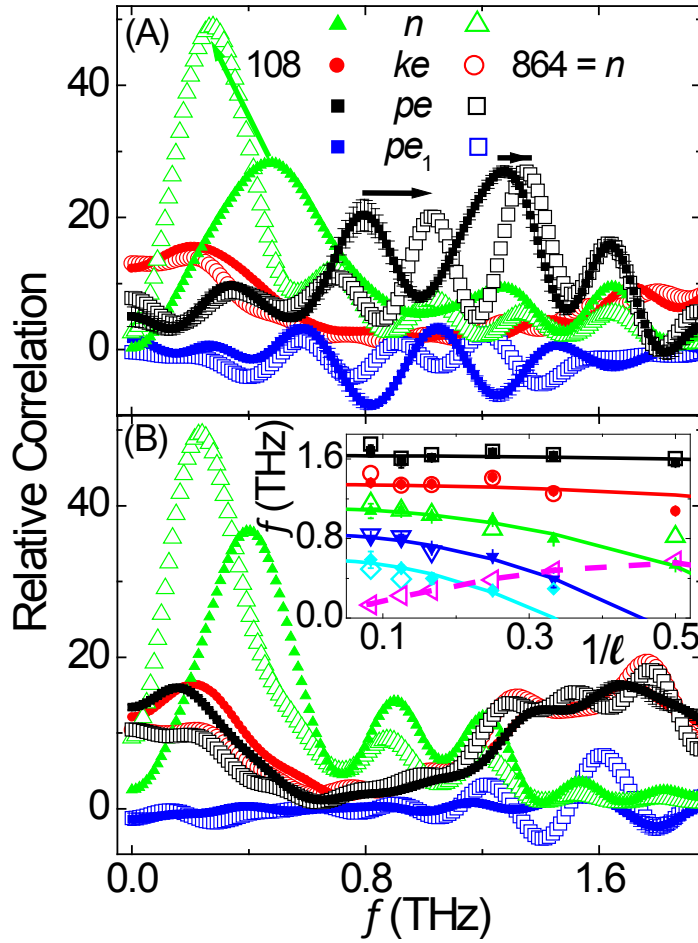


FIG. 5. (Color online) Frequency-dependent correlations in the L-J model from simulations with interaction cutoff radii of $r_c=2.0$ (A) and $r_c=1.5$ (B). Symbols come from the Fourier transform of the normalized autocorrelations in atom density (green triangles), ke (red circles) and pe (black squares). Blue squares show correlations in pe between 1st-neighbor blocks ($j=1$ in Fig 4). Each spectrum comes from averaging behavior from blocks containing an exact number of atoms $n=108$ (solid symbols) or $n=864$ (open symbols), except for fluctuations in n which were obtained by shifting the block positions to align with the equilibrium atomic planes so that n fluctuates as atoms move. Each spectrum also involves averaging from three temperatures ($kT/\varepsilon = 0.0005, 0.001, \text{ and } 0.002$), with error bars for the solid squares (visible when larger than the symbol size). Arrows in (A) indicate how three normal modes (peaks) shift when the block size is changed. Only fluctuations in n show such distinct peaks in the robustly harmonic lattice, (B). Symbols in the inset of (B) show the $1/l$ dependence of the peaks from (A) for the pe correlations (solid) and n correlations (open), with lines from fits to the data using a sine function (dashed) or quadratic function (solid), see text.

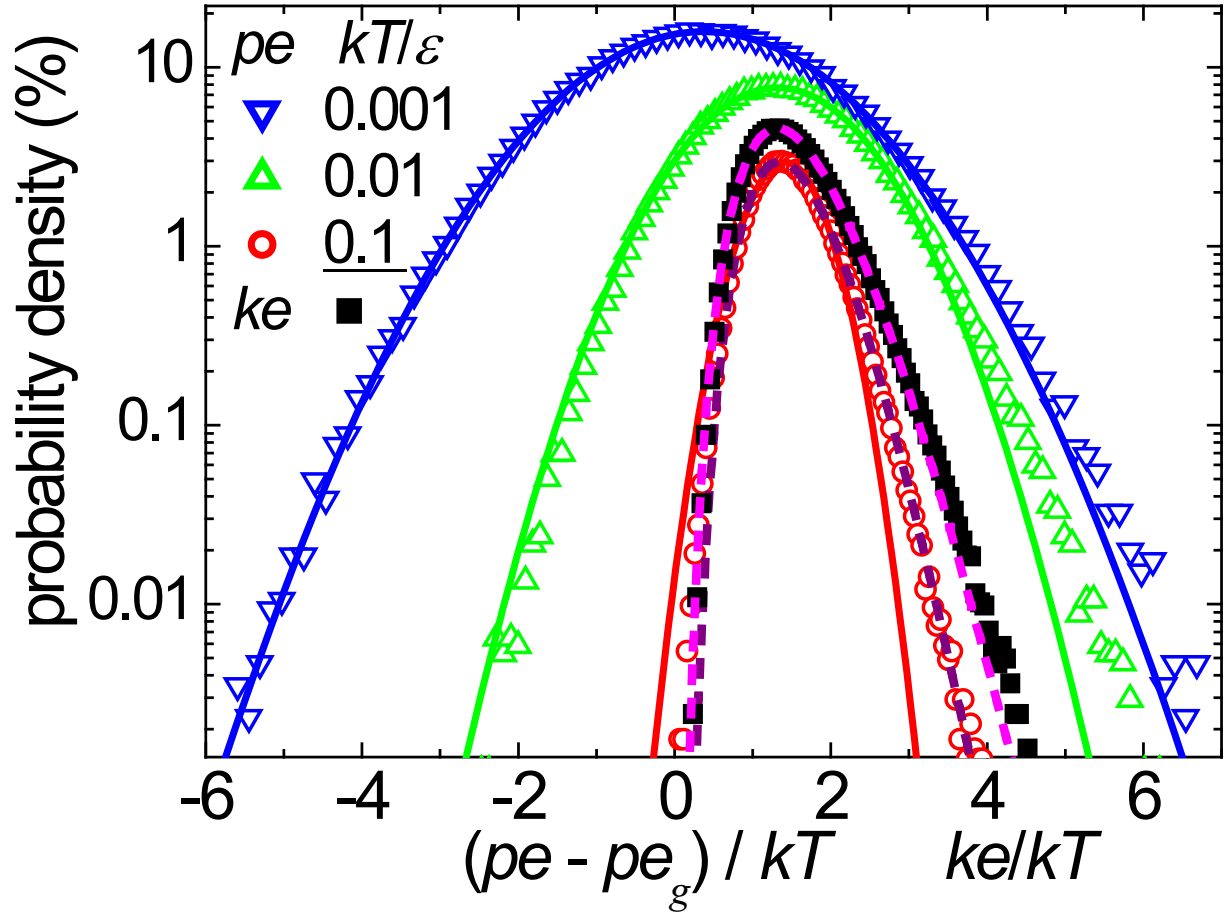


FIG. 6. (Color online) Probability densities for energies in small blocks ($\langle n \rangle = 4.0 \pm 0.5$) as a function of reduced energy from simulations of the L-J model at T given in the legend. Open symbols show pe probabilities as a function of $(pe - pe_g)/kT$, where pe_g is the ground state energy as $T \rightarrow 0$. For clarity, these probabilities were multiplied by factors of 0.5, 2, and 4 for $kT/\varepsilon = 0.1, 0.01$, and 0.001 , respectively; while for $kT/\varepsilon = 0.001$ the horizontal axis was multiplied by a factor of 0.5. Solid lines show Gaussian fits to these pe probabilities. Solid squares show ke probabilities as a function of ke/kT . Dividing by kT removes the temperature dependence of ke , with error bars smaller than the symbol size. Dashed lines show fits to this ke probability, and to the pe probability at $kT/\varepsilon = 0.1$, using the equilibrium canonical-ensemble expression for a finite number of ideal-gas particles, $(AE/kT)^\alpha e^{-BE/kT}$.